

High-Efficiency Generation of Airy Beams with Huygens' Metasurface

Weiming Hao,¹ Ming Deng,¹ Shuqi Chen,^{2,*} and Lin Chen^{1,†}

¹ Wuhan National Laboratory for Optoelectronics, Huazhong University of Science and Technology, Wuhan 430074, China

² Laboratory of Weak Light Nonlinear Photonics Ministry of Education School of Physics, Teda Applied Physics Institute, Nankai University, Tianjin 300071, China



(Received 26 January 2019; revised manuscript received 12 April 2019; published 6 May 2019)

Metasurfaces have shown great potential to generate Airy beams, but the available schemes with dielectric and plasmonic metasurfaces suffer from a lack of amplitude modulation and/or low transmission efficiency. Huygens' metasurfaces have the capability of manipulating electromagnetic wave fronts without reflection, and hence have offered a robust approach to exploit empowered functionalities, such as reflecting, refracting, and focusing plane waves. Here we propose a Huygens' metasurface structure comprised of a metal capacitor sandwiched between double-pair U-shaped ring resonators, which is capable of independently controlling the electric and magnetic dipole responses. The electric admittance and magnetic impedance can be tuned within a wide range, which enables us to achieve nearly arbitrary transmission amplitude and phase for the transmitted waves. The meta-atom of Huygens' metasurface can be designed to have ultrahigh transmission amplitude (nearly 100% for the maximum value), and the resultant Airy-beam generators assembled with the Huygens' metasurfaces present high transmission efficiency. We theoretically design transmissive Airy-beam generators that require polynary amplitude and binary phase distributions, and experimentally verify their excellent performances in terms of transmission efficiency. Our results, based on the independent control of electric admittance and magnetic impedance, can stimulate making high-efficiency wave-front manipulation devices with diversified functionalities in different frequency domains.

DOI: 10.1103/PhysRevApplied.11.054012

I. INTRODUCTION

Metasurfaces, two-dimensional equivalent of metamaterials, have recently shown an unprecedented approach to the extreme control of the reflective and transmissive properties of electromagnetic (EM) waves [1,2]. Metasurfaces utilize interfacial phase discontinuities introduced by subwavelength-sized planar resonators to locally control the amplitude and phase of scattered waves and thus to reshape the wave front of EM waves, leading to a variety of intriguing phenomena and applications such as light bending [3], unidirectional surface-plasmon coupling [4], invisibility [5,6], flat lenses [7–9], holography [10,11], generation of vortex beam [3], and achromatic optics lens [12–15]. Benefiting from the flexibility of modulating the amplitude and phase of EM waves, metasurfaces have also been extensively used to generate various complex field distributions, such as Airy beams [16–21], which typically need to introduce complicated amplitude and phase distributions. The dielectric metasurface Airy-beam generators have the advantage of realizing high transmission

[16], but the available metadevices inevitably suffer from limited nondiffracting propagation distance due to a lack of amplitude modulation. While promising steps have been taken to generate Airy beams with simultaneous amplitude and phase modulation with single-layer plasmonic metasurface [17–21], the transmission efficiency is highly limited because of intrinsically low transmission amplitude for a plasmonic meta-atom.

Huygens' metasurfaces (HMSs) have offered a promising approach to construct high-efficiency transmissive metadevices by generating orthogonal equivalent electric and magnetic currents to exquisitely control the scattering fields for specific EM response [22]. A noticeable feature of a HMS meta-atom is that nearly 100% transmission amplitude is possible, hence representing a promising avenue to tackle the challenge faced by plasmonic metasurfaces. To avoid the plasmonic loss incurred by metals, dielectric HMSs have been widely proposed to address the issue of low working efficiency at high frequencies [23–28]. A large amount of studies on HMSs are focused on phase modulation, while maintaining a high transmission efficiency. By means of independently controlling the amplitude and phase of transmissive waves, HMSs have been successfully designed to expand the practical

*schen@nankai.edu.cn

†chen.lin@mail.hust.edu.cn

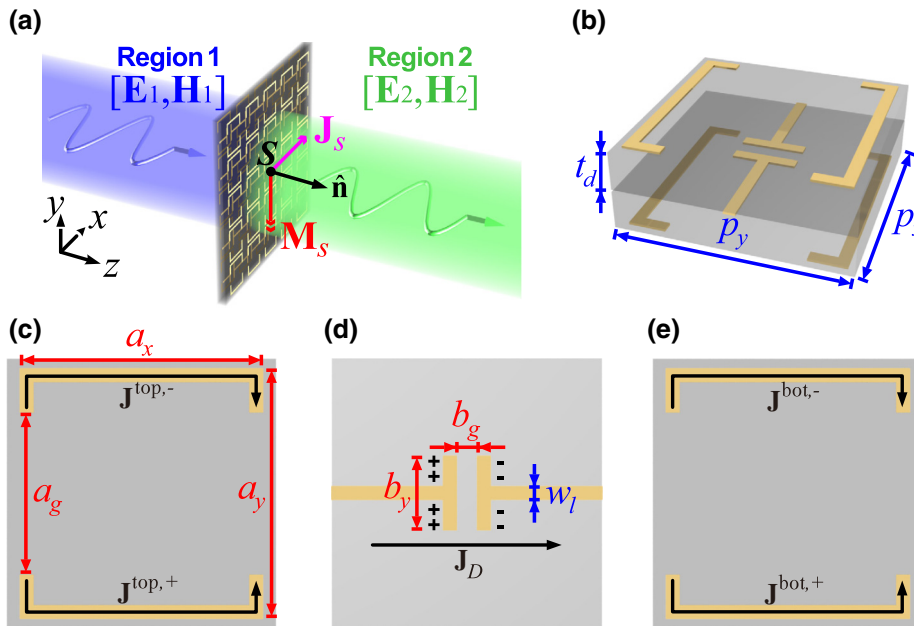
applications such as controlling the diffraction waves [29–32]. While a HMS meta-atom has the capability of modulating amplitude of 0%–100%, associated with 0– 2π phase modulation, realizing high-efficiency Airy beams with HMSs still remains unexplored.

In this paper, we propose a HMS design that is capable of achieving nearly arbitrary transmission amplitude and phase for the transmitted waves. The meta-atom of the HMS, consisting of a metal capacitor sandwiched between double-pair U-shaped ring resonators, is purposely designed to have electric and magnetic dipole responses, respectively. Once the double-pair U-shaped ring resonators are already designed for magnetic dipole response, one can simply design the metal capacitor to tune the electric dipole response with less influence of the magnetic dipole response. As a result, one is able to generate nearly arbitrary transmission amplitude and phase for the transmitted waves with an appropriate design of the HMS units. This thus expands the HMSs' functionalities besides reflecting, refracting, or focusing plane waves, which typically requires uniform transmission-amplitude distributions. The meta-atom of HMS presents ultrahigh transmission amplitude (nearly 100% for the maximum value), and the resultant Airy-beam generators assembled with the HMSs present high transmission efficiency. The concept of HMS Airy-beam generators is demonstrated in the microwave and terahertz domain.

II. RESULTS

A. Operating principle

Figure 1(a) schematically shows the arbitrary EM fields in two regions (regions 1 and 2) separated by a surface element S that offers electric and magnetic surface currents.



Considering the fact that the field intensities are discontinuous at the surface S , the fictitious electric and magnetic surface-current densities \mathbf{J}_S and \mathbf{M}_S are required to follow the boundary conditions as [22]

$$\mathbf{J}_S = \hat{\mathbf{n}} \times (\mathbf{H}_2 - \mathbf{H}_1), \quad (1a)$$

$$\mathbf{M}_S = -\hat{\mathbf{n}} \times (\mathbf{E}_2 - \mathbf{E}_1). \quad (1b)$$

We can use the local equivalent electric admittance tensor, Y_{es} , and magnetic impedance tensor, Z_{ms} , representing the EM properties of HMSs, to link up \mathbf{J}_S and \mathbf{M}_S . We note the effective permittivity and permeability are frequently used to describe EM properties of metamaterials that are treated as a bulk material having a certain thickness. However, it is not suited to correlate them with \mathbf{J}_S and \mathbf{M}_S . In contrast, the equivalent electric admittance and magnetic impedance are suitable for describing the EM response at the interface of two regions. Considering that the HMSs are ultrathin, we can thus use Y_{es} and Z_{ms} to completely represent the EM properties of HMSs. Under the conditions that the incident waves are x polarized and no polarization conversion occurs during the whole process, we can thus merely take $Y_{es,xx}$ and $Z_{ms,yy}$ into consideration. When the HMSs are surrounded by air, $Y_{es,xx}$ and $Z_{ms,yy}$ can be normalized to the wave impedance of free space as

$$Y = Y_{es,xx} \eta = \frac{\mathbf{J}_S \cdot \hat{\mathbf{x}}}{\frac{1}{2}(\mathbf{E}_1 + \mathbf{E}_2) \cdot \hat{\mathbf{x}}} \eta = \frac{2\eta(H_2^y - H_1^y)}{E_1^x + E_2^x}, \quad (2a)$$

$$Z = Z_{ms,yy} \frac{1}{\eta} = \frac{\mathbf{M}_S \cdot \hat{\mathbf{y}}}{\frac{1}{2}(\mathbf{H}_1 + \mathbf{H}_2) \cdot \hat{\mathbf{y}}} \frac{1}{\eta} = \frac{2(E_2^x - E_1^x)}{\eta(H_1^y + H_2^y)}, \quad (2b)$$

FIG. 1. Schematic illustration of the HMS and its working principle. (a) Arbitrary fields in the two regions separated by a surface element S . (b) The meta-atom of the HMS consisting of three-layer metal patterns (one metal capacitor sandwiched between double-pair U-shaped ring resonators), spaced by dielectric layer. (c)–(e) Metallic patterns and induced currents in the TL, ML, and BL for a meta-atom.

where $\hat{\mathbf{x}}$ and $\hat{\mathbf{y}}$ are the unit vector along the x and y directions, respectively, E_1^x and E_2^x , H_1^y and H_2^y are the tangential components of electric and magnetic fields in regions 1 and 2, respectively. According to the generalized sheet transition condition [33], and its derivation [34], the transmission and reflection complex coefficients of surface element S can be written as

$$T = (4 - YZ) / [(2 + Y)(2 + Z)], \quad (3a)$$

$$R = 2(Z - Y) / [(2 + Y)(2 + Z)], \quad (3b)$$

where $T = t \exp(\varphi_t)$ and $R = r \exp(\varphi_r)$ are the transmittance and reflectance, $t(\varphi_t)$, and $r(\varphi_r)$ are the transmission and reflection amplitude (phase), respectively. If the absorptivity of the HMSs is negligible, Y and Z are pure imaginary values, and hence $|T|^2 + |R|^2 = 1$. Further, if Y is equal to Z , the HMSs are reflectionless, which has been widely used to enable high-performance wave-front manipulation [22–28]. In addition, we note arbitrary electric admittance and magnetic impedance have been previously employed in HMSs to introduce nonuniform scattered-field distributions to control the diffracted field [29–32].

Figure 1(b) schematically shows the proposed meta-atom of the HMS consisting of a metal capacitor sandwiched between double-pair U-shaped ring resonators. The three-layer metallic patterns, i.e., top layer (TL), middle layer (ML), and bottom layer (BL), are presented in Figs. 1(c)–1(e). Compared with commonly used single metal strip and double metal strips, the metal capacitor and double-pair U-shaped ring can reduce the size of the meta-atom, which thus increases the number of sampling dots, and hence benefits sampling accuracy. In addition, they can avoid the cross-polarization conversion, owing to their mirror symmetries to the x axis and y axis. Once such meta-atom is illuminated with x -polarized EM waves, the surface currents are induced in the three layers, denoted as \mathbf{J}^{top} , \mathbf{J}^{mid} and \mathbf{J}^{bot} , respectively. The induced

currents in the TL or BL are the sum of conduction currents in the two opposite U-shaped rings, while the induced current in the ML comes from the displacement current across the capacitor

$$\mathbf{J}^{\text{top}} = \mathbf{J}^{\text{top},+} + \mathbf{J}^{\text{top},-}, \quad (4a)$$

$$\mathbf{J}^{\text{mid}} = \mathbf{J}_D, \quad (4b)$$

$$\mathbf{J}^{\text{bot}} = \mathbf{J}^{\text{bot},+} + \mathbf{J}^{\text{bot},-}. \quad (4c)$$

The surface currents in the three layers are presented in detail in Note 1 within the Supplemental Material [35]. We find that a meta-atom can support one magnetic dipole, associated with the resonance frequency f_M , and two electric dipoles, associated with two resonance frequencies, f_{E1} and f_{E2} , respectively. We conduct the finite-difference time domain (FDTD) method using commercial software *Lumerical FDTD Solutions* to model the EM response of the HMS presented in Fig. 1(b). The electric admittance, Y , and magnetic impedance, Z , are retrieved by incorporating the transmission and reflection coefficients into Eq. (3). The geometrical parameters used for the simulations are $p_x = p_y = 4$ mm, $t_d = 1$ mm, $w_l = 0.2$ mm, and $a_y = 3.7$ mm (all are fixed in this work), and, a_g , a_x , b_g , and b_y (are variable in the following work) is 1.2, 2.2, 0.3, 2.0 mm. The thickness of each metal (copper) pattern is 0.017 mm. The conductivity of cooper is set as $5 \times 10^7 \Omega^{-1} \text{ m}^{-1}$, and the relative permittivity of the FR4 layer is set as $4.3 + 0.05i$. It can be seen from Fig. 2(a) that three resonance frequencies occur in the frequency range of interest, associated with f_{E1} , f_M , and f_{E2} mentioned above. As a comparison, we can see that, f_M , associated with the magnetic response, is unchanged, while f_{E1} vanishes and f_{E2} is slightly shifted without the involvement of the ML [Fig. 2(b)]. Both f_M and f_{E2} vanish and f_{E1} undergoes a shift when we remove the TL and the BL [Fig. 2(c)]. The comparative study presented here verifies that the coupling between the TL (BL) and ML, contributes to the two electric responses, and hence f_{E1} and f_{E2} can

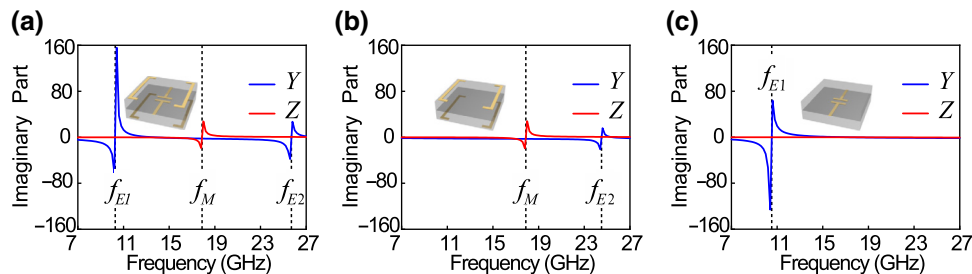


FIG. 2. Imaginary parts of Y and Z versus frequencies. (a) One magnetic response (f_M) and two electric responses (f_{E1} and f_{E2}) occur as both the metal capacitor and double-pair U-shaped ring resonators are used. (b) The magnetic response (f_M) is unchanged, while f_{E1} vanishes and f_{E2} is slightly shifted with the absence of the metal capacitor. (c) Merely f_{E1} is left with the absence of the double-pair U-shaped ring resonators. The structural parameters used for the metallic patterns are $a_g = 1.2$ mm, $a_x = 2.2$ mm, $b_g = 0.3$ mm, and $b_y = 2.0$ mm.

be slightly shifted. Meanwhile, the magnetic response suffers little from the coupling, and hence f_M is unchanged. More simulation results demonstrate that the ML significantly affects the electric response, but does not influence the magnetic response at all, even if the thickness of the dielectric spacer experiences a large variation (see more details in Note 2 within the Supplemental Material [35]).

B. Design of the building block and Airy-beam generator

We aim to design a meta-atom of a HMS [Fig. 1(b)] that is capable of achieving nearly arbitrary transmission amplitude and phase for the transmitted waves. Understanding the EM response mentioned in the above section helps us with the design. We should first design a_g and a_x to determine f_M so as to fix the Z , associated with the magnetic response. In this way, we can simply modulate the geometrical parameters of the ML (b_g and b_y) to control f_{E1} and f_{E2} so as to flexibly tune the Y , associated with the electric response, without shifting f_M . These two design steps are intended to make both Z and Y vary within a wide range so that arbitrary transmission amplitude and phase distributions are expected. Figure 3 illustrates that nearly arbitrary transmission amplitude and phase distributions are realized as Z and Y range from $(-10i, 10i)$. Considering the practical structure shown in Fig. 1(b) where the absorption loss is so small due to the involvement of the FR4 layer, the Z and Y can be treated as pure imaginary values. We can thus achieve the required transmission amplitude and phase distributions for the particular wave-front manipulation. As an example, we design two groups of meta-atoms whose transmission phases have a difference of π , while their transmission amplitudes vary within the range of 0 to 1 [Fig. 4]. The geometrical parameters, Z and Y , retrieved from Eq. (3) can be found in Table SI and Fig. S3 of Note 3 within the Supplemental Material [35].

The arbitrarily controlled transmission amplitude and phase with the presented HMS in Fig. 1(b) is applicable to the construction of practical functional devices that require complex transmission coefficients. It should be

noted here, much effort has been previously devoted to exploring HMSs to manipulate light wave front such as reflection, refraction, focusing of light, as well as manipulating the diffracted fields [22–32]. However, there is little work targeted towards generating Airy beams using HMSs, although plenty of work on Airy beams has been demonstrated with single-layered plasmonic and dielectric metasurfaces [16–21]. Airy beam is an analogy to Airy wave-packet solution for a free particle derived from the free-particle Schrödinger equation in electromagnetism [36–38]. As one type of nondiffracting wave, Airy beams have many unique features, including nondiffracting, self-bending [38], and self-healing [39], which stimulate enormous potential applications such as curved plasma-channel generation [40], particle manipulation [39], and light bullet [41,42]. The electric field envelope of a finite energy Airy beam can be described as [37]

$$U(\xi, s) = A \cdot \text{Ai} \left[s - \left(\frac{\xi}{2} \right)^2 + i(\alpha\xi) \right] \exp \left[\alpha s - \frac{\alpha\xi^2}{2} - i \left(\frac{\xi^3}{12} \right) + i \left(\frac{\alpha^2\xi}{2} \right) + i \left(\frac{s\xi}{2} \right) \right], \quad (5)$$

where A and Ai represent the amplitude factor of electric field and Airy function, respectively, and the exponential part indicates the decaying feature. The parameter α is the decay factor, and $s = (x - x_0)/w$ is the dimensionless normalized transverse coordinate, where x is the real laboratory coordinate, x_0 is the reference coordinate for normalization, and w represents the scaling length. $\xi = z/(k_0 w^2)$ is the propagation length normalized by Rayleigh distance, where k_0 is the wave number in free space. The initial field envelope of Airy beam is given by the condition $\xi = 0$ as

$$U_0(x) = U(0, x) = A \cdot \text{Ai} \left(\frac{x - x_0}{w} \right) \exp \left[\alpha \left(\frac{x - x_0}{w} \right) \right], \quad (6)$$

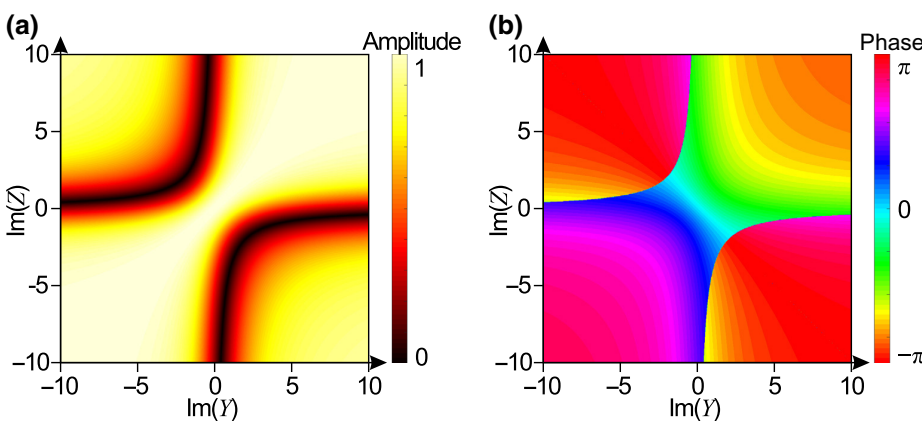


FIG. 3. Local transmission amplitudes (a) and phases (b) as a function of the purely imaginary value of Y and Z .

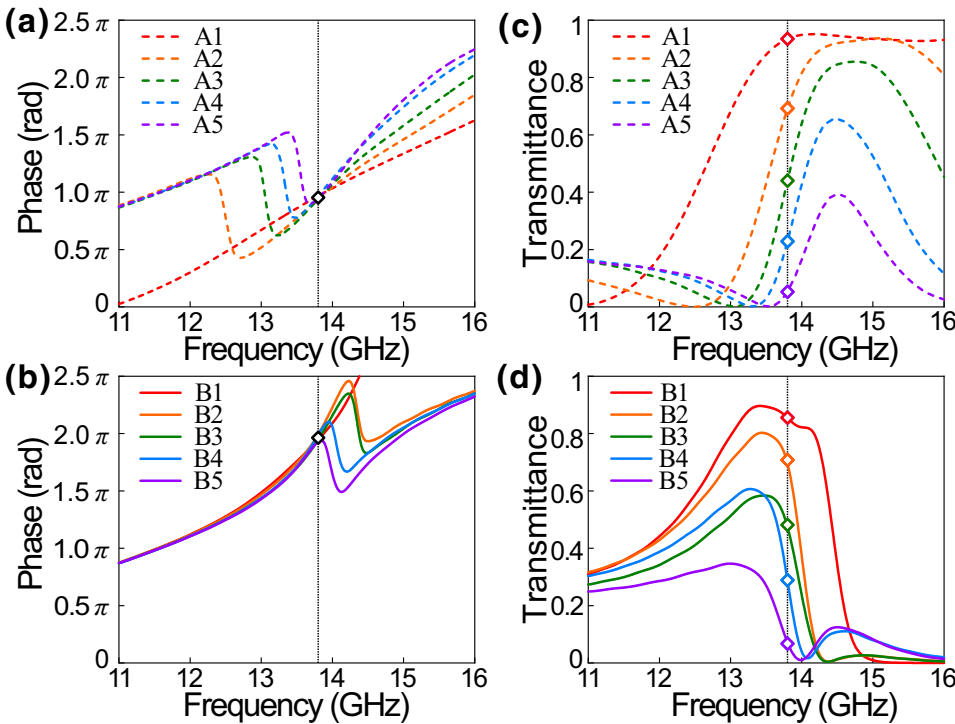


FIG. 4. Two groups of meta-atoms undergo a π difference, while their transmittance varies within the range of 0 to 1. (a),(b) Transmission phases and transmittance of meta-atoms in group A. (c),(d) Transmission phases and transmittance of meta-atoms in group B.

where $U_0(x)$ is a real-value function, in which the initial phase experiences a difference of π as $U_0(x)$ is altered from positive to negative value. To maximize the efficiency of the Airy-beam generator, one should properly select A to satisfy $|U_0(x)|_{\max} = A_{\text{in}}$, where A_{in} is the amplitude of the incident plane waves.

To design practical Airy-beam generators with the present HMSs, 60 units of meta-atoms are used along the x direction, while it is assumed that the HMSs along the y direction are uniform and sufficiently long. Specifically, two sets of parameters $(w, x_0) = (24, 216 \text{ mm})$ and $(21.7, 218.3 \text{ mm})$ with $\alpha = 0.0001$ are employed to construct the Airy-beam generators at 13.8 GHz. The geometrical parameters of the used HMSs, together with their Z and Y retrieved from Eq. (3), can be found in Table SII and Fig. S4 of Note 4 within the Supplemental Material [35], where the blue circles represent the samplings in Figs. 5(a) and 5(b). In the frequency range of interest (7–17 GHz), only the electric resonance, associated with f_{E1} , and the magnetic resonance, associated with f_M , are excited simultaneously. The electric resonance, associated with f_{E2} , is far from the operating frequency, and hence its contribution to Z and Y is negligible. Figures 5(c) and 5(d) show the ideal field intensity distributions for the two designs, retrieved via analytical method with Eq. (5). Figures 5(e) and 5(f) present the simulated field intensity distributions when the designed HMSs are involved. To verify the analyzed and simulated prediction, we implement standard printed circuit-board technology to fabricate realistic samples with 49 units being used along the y direction,

and characterized their device performance with near-field scanning experiment. A part of the fabricated sample one is schematically shown in Fig. 5(i) and the experimental setup is illustrated in Figs. 5(j) and 5(k). The near-field distributions are measured via a R&S ZVL13 vector network analyzer, and the distance between the source and the sample is $L_s = 2500 \text{ mm}$ [Fig. 5(j)]. The experimental results shown in Figs. 5(g) and 5(h) are basically consistent with the simulated results in Figs. 5(e) and 5(f). We note there are limited side lobes presented in the simulation and experiment, compared to the analyzed results in Figs. 5(c) and 5(d). The main reason that causes the difference arises from the finite units of HMS used along the x direction in the simulation and experiment. The deviation between the simulated and measured results come from the fabrication error and finite distance L_s between the horn antenna (as the source) and sample. We have noted in the recent study on Airy beams with plasmonic metasurfaces [17–20], the transmission efficiencies of Airy beams, defined as the ratio of the maximum electric field intensity of output beam to that of the incident light [19], are all far below 1 [17–20]. As for the present case, the transmission efficiencies, where the electric field intensity is extracted at $z = 66 \text{ mm}$ (around threefold wavelengths) away from HMSs, are 1.18 and 0.98 for the two designed generators. The present results indicate that the HMS scheme could significantly increase the transmission efficiency, compared to those with plasmonic metasurfaces.

The self-healing feature of an Airy beam is usually verified by placing a scatterer on the travelling path of

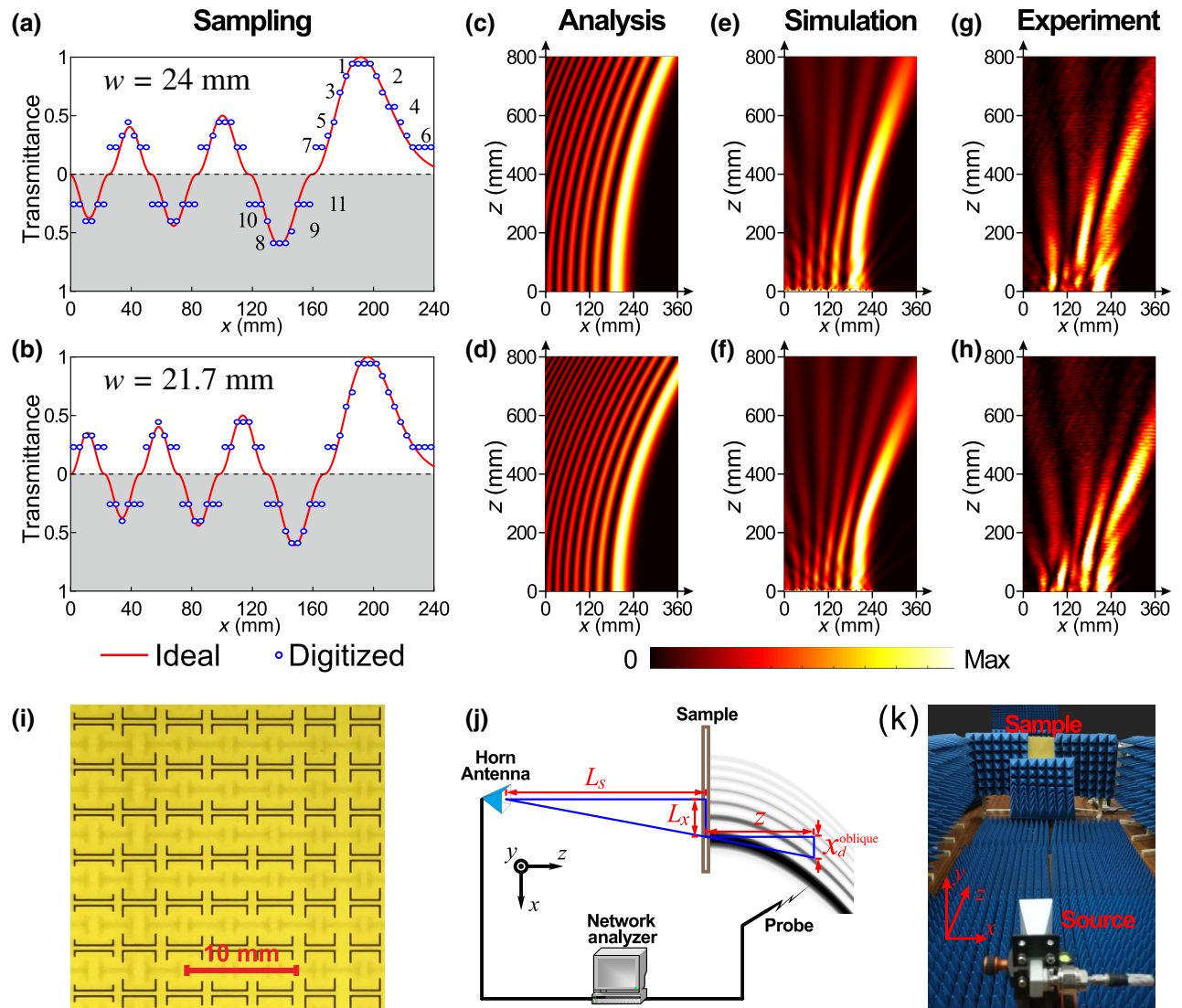


FIG. 5. Experimental verification of HMS Airy-beam generators. (a),(b) Transmittance distributions along the x direction. Blue circles represent the sampling points and red solid lines stand for the transmittance distributions required by the field envelop of the Airy beam. (c)–(h) Field intensity distributions of output fields with analytical method (c),(d), according to Eq. (5), full-wave simulation (e),(f), and experiment (g),(h). (i) A part of the fabricated sample. (j),(k) Near-field scanning experiment setup.

the main lobe. Here we numerically demonstrate that the main lobe can still recover after placing a perfect electric conductor (PEC) of $16 \times 20 \text{ mm}^2$ in size (70 mm away from the sample) on the path of the main lobe [see Figs. S5(a) and S5(b) in Note 5 within the Supplemental Material [35]]. In addition, nondiffraction and self-bend are the two other features of an Airy beam, and the measurable indicators of them are the variation of the FWHM and the deflection offset of the main lobe, respectively. The FWHM is oscillating around the predesigned values of 39.20 and 35.42 mm, respectively, as the propagation distance is below 20-fold wavelengths [see Figs. S2(c) and S2(d) in Note 5 within the Supplemental Material [35]]. These values are further enhanced as the propagation distance increases but are kept below 1.5 times the

predesigned values (39.20 and 35.42 mm), even if the propagation distance reaches 28- and 24-fold wavelengths. We also investigate the self-bending characteristic of the Airy beams, and the experimental and simulated results are basically consistent with the theoretical prediction [see Figs. S5(e) and S5(f) and the accompanied discussions in Note 5 within the Supplemental Material [35]].

C. Extension to terahertz frequencies

The design strategy to generate arbitrary transmission amplitude and phase using a meta-atom of the HMS is so general that we can also employ it in higher-frequency domains. As an illustration, we extend the working frequencies to terahertz frequencies. The meta-atom of the

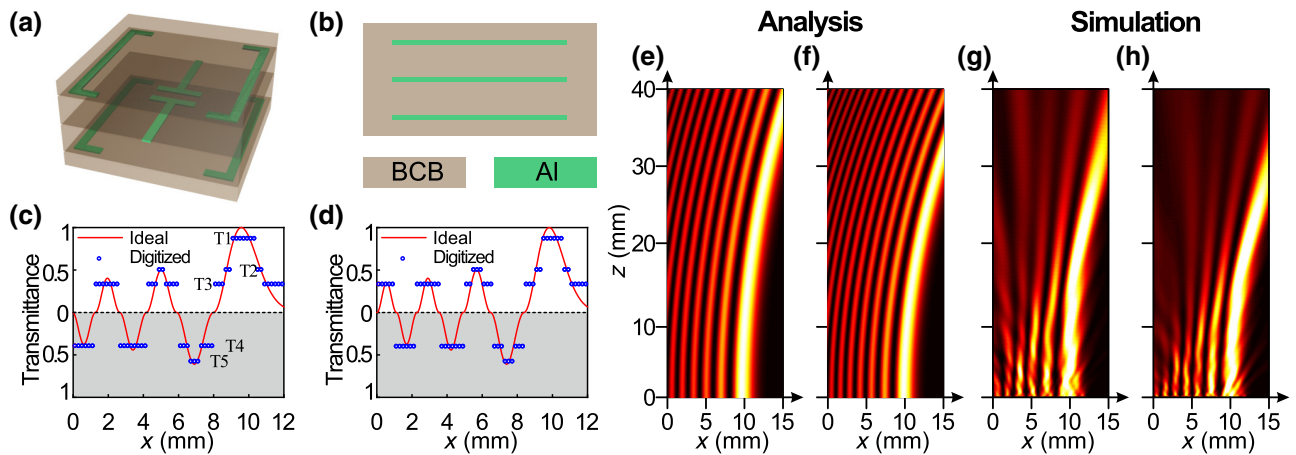


FIG. 6. Numerical demonstration of the Airy-beam generators at 0.3 THz. (a),(b) Schematic of a meta-atom (group T), with p_x , p_y , a_y , and w_l fixed at $p_x = p_y = 0.2$ mm, $a_y = 0.185$ mm, and $w_l = 0.01$ mm. The other variables are listed in Table SIII of Note 6 within the Supplemental Material [35]. (c),(d) Transmittance distributions along the x direction. Blue circles represent the sampling points and red solid lines stand for the transmittance distributions required by the field envelop of Airy beams. (e)–(h) Field intensity distributions of output fields with analytical method (e),(f) according to Eq. (5), and full-wave simulation (g),(h). In the modeling, α is set as 0.0001, (w, x_0) are (1.2, 10.8 mm) in (c), (e), and (g), and (1.086, 10.914 mm) in (d), (f), and (h).

HMS is schematically presented in Fig. 6(a), with the side-view schematic being shown in Fig. 6(b). We chose aluminum (Al) as the metallic material and benzocyclobutene (BCB) as the dielectric spacer between the metal patterns. Different from the HMS used in the microwave domain, we introduce a BCB substrate to support the HMS, and then use a BCB cladding layer (with the same thickness of coating) to cover the HMS, for eliminating the bianisotropy. The thicknesses of each metal layer, each BCB spacer, and cladding and substrate layer are 200 nm, 60 μ m, and 20 μ m, respectively. The relative permittivity of the Al layer is obtained by fitting the experimental data to the well-known Drude model $\epsilon_\omega = 1 - \omega_p^2/\omega(\omega - i\omega_\tau)$, where ω is the angular frequency, ω_p and ω_τ are 3570 and 19.4 THz, respectively [43]. The relative dielectric constant and loss tangent of the BCB layer are 2.45 and 0.01, extracted from an experiment reference [44]. It should be noted here, the conductivity of Al is still a very large value, and BCB, as a typically used dielectric material, has an ultralow loss in the terahertz domain. It can thus be reasonably inferred that, the absorption loss of the meta-atom presented in Fig. 6(a), arising from material loss of Al and BCB can be ignored. Previous experimental results in the terahertz region have proven the low-loss absorption as Al and BCB are involved [45,46]. The BCB layers can be obtained with spin-coating technique, and the metallic pattern can be precisely formed by use of optical lithography, followed by deposition techniques such as magnetron sputtering deposition or electron beam evaporation. The alternative Al and BCB layers can be formed by repeating the above process on a back plate. Finally, the HMS Airy-beam generator can be obtained by removing the back plate by wet etching [47]. Figures 6(c) and 6(d) present

two groups of transmission distributions versus x coordinate at 0.3 THz, where the corresponding phase shift experiences alternative π . The detailed structural parameters for the metal patterns can be found in Table SIII of Note 6 within the Supplemental Material [35]. By arranging these meta-atoms along the x direction to enable the transmission amplitude and phase distributions required by the field envelope of the Airy beam, one can thus construct the Airy-beam generator at terahertz frequencies. The simulated electric field intensity distributions are shown in Figs. 6(g) and 6(h), which are in accordance with the theoretical analysis in Figs. 6(e) and 6(f). The transmission efficiency for the two designed generators are 1.20 and 1.11, extracted at $z = 3.0$ mm (around threefold wavelengths) away from HMSs.

III. CONCLUSION

To summarize, we design a building block of HMS that can be used to independently control the electric and magnetic dipole responses. The HMSs show the advantages of introducing nearly arbitrary transmission amplitude (0%–100%) and phase for the transmitted waves. This thus extends the functionalities of previous HMSs that are purposely designed to reflect, refract, or focus EM waves. As a proof-of-concept demonstration, we design a series of transmissive meta-atoms appearing as polynary amplitude and binary-phase distributions. By arranging these meta-atoms to follow the field envelope of the Airy beam, we show that the assembled structures present the capability of generating Airy beams with high transmission efficiency. Such HMSs can be easily extended to higher frequencies as well as scaling down the structural parameters, and we

employ full wave simulations to demonstrate the generation of Airy beams at terahertz frequencies. The HMS strategy is proven capable of increasing the transmission efficiency of Airy-beam generation, with approximately 1 both in the microwave and teratherz frequencies, superior over the previously reported plasmonic-metasurface scheme in the terahertz region. Our findings can inspire the design of high-performance photonic components for particular wave-front manipulation applications with the requirement of flexibly tuning the transmission amplitude and phase simultaneously.

ACKNOWLEDGMENTS

This work was supported by National Natural Science Foundation of China (Grant Nos. 11474116, 11674118, 11774186) and State Key Laboratory of Advanced Technology for Materials Synthesis and Processing (Wuhan University of Technology).

-
- [1] H.-T. Chen, A. J. Taylor, and N. Yu, A review of metasurfaces: physics and applications, *Rep. Prog. Phys.* **79**, 076401 (2016).
- [2] N. Yu and F. Capasso, Flat optics with designer metasurfaces, *Nat. Mater.* **13**, 139 (2014).
- [3] N. Yu, P. Genevet, M. A. Kats, F. Aieta, J.-P. Tetienne, F. Capasso, and Z. Gaburro, Light propagation with phase discontinuities: Generalized laws of reflection and refraction, *Science* **334**, 333 (2011).
- [4] J. Lin, J. P. B. Mueller, Q. Wang, G. Yuan, N. Antoniou, X.-C. Yuan, and F. Capasso, Polarization-controlled tunable directional coupling of surface plasmon polaritons, *Science* **340**, 331 (2013).
- [5] X. Ni, Z. J. Wong, M. Mrejen, Y. Wang, and X. Zhang, An ultrathin invisibility skin cloak for visible light, *Science* **349**, 1310 (2015).
- [6] X. Kong, J. Xu, J.-j. Mo, and S. Liu, Broadband and conformal metamaterial absorber, *Front. Optoelectron.* **10**, 124 (2017).
- [7] M. Khorasaninejad, A. Y. Zhu, C. Roques-Carmes, W. T. Chen, J. Oh, I. Mishra, R. C. Devlin, and F. Capasso, Polarization-insensitive metalenses at visible wavelengths, *Nano Lett.* **16**, 7229 (2016).
- [8] X. Yin, H. Zhu, H. Guo, M. Deng, T. Xu, Z. Gong, X. Li, Z. H. Hang, C. Wu, H. Li, S. Chen, L. Zhou, and L. Chen, Hyperbolic metamaterial devices for wavefront manipulation, *Laser Photonics Rev.* **13**, 1800081 (2019).
- [9] T. Yang, H. Lin, and B. Jia, Two-dimensional material functional devices enabled by direct laser fabrication, *Front. Optoelectron.* **11**, 2 (2018).
- [10] X. Ni, A. V. Kildishev, and V. M. Shalaev, Metasurface holograms for visible light, *Nat. Commun.* **4**, 2807 (2013).
- [11] G. Zheng, H. Mühlenbernd, M. Kenney, G. Li, T. Zentgraf, and S. Zhang, Metasurface holograms reaching 80% efficiency, *Nat. Nanotechnol.* **10**, 308 (2015).
- [12] E. Arbabi, A. Arbabi, S. M. Kamali, Y. Horie, and A. Faraon, Controlling the sign of chromatic dispersion in diffractive optics with dielectric metasurfaces, *Optica* **4**, 625 (2017).
- [13] S. Wang, P. C. Wu, V.-C. Su, Y.-C. Lai, C. Hung Chu, J.-W. Chen, S.-H. Lu, J. Chen, B. Xu, C.-H. Kuan, T. Li, S. Zhu, and D. P. Tsai, Broadband achromatic optical metasurface devices, *Nat. Commun.* **8**, 187 (2017).
- [14] W. T. Chen, A. Y. Zhu, V. Sanjeev, M. Khorasaninejad, Z. Shi, E. Lee, and F. Capasso, A broadband achromatic metalens for focusing and imaging in the visible, *Nat. Nanotechnol.* **13**, 220 (2018).
- [15] S. Wang, P. C. Wu, V.-C. Su, Y.-C. Lai, M.-K. Chen, H. Y. Kuo, B. H. Chen, Y. H. Chen, T.-T. Huang, J.-H. Wang, R.-M. Lin, C.-H. Kuan, T. Li, Z. Wang, S. Zhu, and D. P. Tsai, A broadband achromatic metalens in the visible, *Nat. Nanotechnol.* **13**, 227 (2018).
- [16] Q. Fan, D. Wang, P. Huo, Z. Zhang, Y. Liang, and T. Xu, Autofocusing Airy beams generated by all-dielectric metasurface for visible light, *Opt. Express* **25**, 9285 (2017).
- [17] S. Wang, X. Wang, and Y. Zhang, Simultaneous Airy beam generation for both surface plasmon polaritons and transmitted wave based on metasurface, *Opt. Express* **25**, 23589 (2017).
- [18] J. He, S. Wang, Z. Xie, J. Ye, X. Wang, Q. Kan, and Y. Zhang, Abruptly autofocusing terahertz waves with metahologram, *Opt. Lett.* **41**, 2787 (2016).
- [19] E. Y. Song, G. Y. Lee, H. Park, K. Lee, J. Kim, J. Hong, H. Kim, and B. Lee, Compact generation of Airy beams with C-aperture metasurface, *Adv. Opt. Mater.* **5**, 1601028 (2017).
- [20] Z. Li, H. Cheng, Z. Liu, S. Chen, and J. Tian, Plasmonic Airy beam generation by both phase and amplitude modulation with metasurfaces, *Adv. Opt. Mater.* **4**, 1230 (2016).
- [21] J. Ding, S. An, B. Zheng, and H. Zhang, Multiwavelength metasurfaces based on single-layer dual-wavelength meta-atoms: Toward complete phase and amplitude modulations at two wavelengths, *Adv. Opt. Mater.* **5**, 1700079 (2017).P
- [22] C. Pfeiffer and A. Grbic, Metamaterial Huygens' Surfaces: Tailoring Wave Fronts with Reflectionless Sheets, *Phys. Rev. Lett.* **110**, 197401 (2013).
- [23] A. J. Ollanik, J. A. Smith, M. J. Belue, and M. D. Escarra, High-efficiency all-dielectric Huygens metasurfaces from the ultraviolet to the infrared, *ACS Photonics* **5**, 1351 (2018).
- [24] K. E. Chong, L. Wang, I. Staude, A. R. James, J. Dominguez, S. Liu, G. S. Subramania, M. Decker, D. N. Neshev, I. Brener, and Y. S. Kivshar, Efficient polarization-insensitive complex wavefront control using Huygens' metasurfaces based on dielectric resonant meta-atoms, *ACS Photonics* **3**, 514 (2016).
- [25] K. E. Chong, I. Staude, A. James, J. Dominguez, S. Liu, S. Campione, G. S. Subramania, T. S. Luk, M. Decker, D. N. Neshev, I. Brener, and Y. S. Kivshar, Polarization-independent silicon metadevices for efficient optical wavefront control, *Nano Lett.* **15**, 5369 (2015).
- [26] S. Liu, A. Vaskin, S. Campione, O. Wolf, M. B. Sinclair, J. Reno, G. A. Keeler, I. Staude, and I. Brener, Huygens' metasurfaces enabled by magnetic dipole resonance tuning in split dielectric nanoresonators, *Nano Lett.* **17**, 4297 (2017).

- [27] C. Pfeiffer, N. K. Emani, A. M. Shaltout, A. Boltasseva, V. M. Shalaev, and A. Grbic, Efficient light bending with isotropic metamaterial Huygens' surfaces, *Nano Lett.* **14**, 2491 (2014).
- [28] L. Zhang, J. Ding, H. Zheng, S. An, H. Lin, B. Zheng, Q. Du, G. Yin, J. Michon, Y. Zhang, Z. Fang, M. Y. Shalaginov, L. Deng, T. Gu, H. Zhang, and J. Hu, Ultra-thin high-efficiency mid-infrared transmissive Huygens meta-optics, *Nat. Commun.* **9**, 1481 (2018).
- [29] S. L. Jia, X. Wan, D. Bao, Y. J. Zhao, and T. J. Cui, Independent controls of orthogonally polarized transmitted waves using a Huygens metasurface, *Laser Photonics Rev.* **9**, 545 (2015).
- [30] A. Epstein, J. P. S. Wong, and G. V. Eleftheriades, Cavity-excited Huygens' metasurface antennas for near-unity aperture illumination efficiency from arbitrarily large apertures, *Nat. Commun.* **7**, 10360 A. J. (2016).
- [31] X. Wan, S. L. Jia, T. J. Cui, and Y. J. Zhao, Independent modulations of the transmission amplitudes and phases by using Huygens metasurfaces, *Sci. Rep.* **6**, 25639 (2016).
- [32] X. Wan, L. Zhang, S. L. Jia, J. Y. Yin, and T. J. Cui, Horn antenna with reconfigurable beam-refraction and polarization based on anisotropic Huygens metasurface, *IEEE Trans. Antennas Propag.* **65**, 4427 (2017).
- [33] E. F. Kuester, M. A. Mohamed, M. Piket-May, and C. L. Holloway, Averaged transition conditions for electromagnetic fields at a metafilm, *IEEE Trans. Antennas Propag.* **51**, 2641 (2003).
- [34] C. L. Holloway, M. A. Mohamed, E. F. Kuester, and A. Dienstfrey, Reflection and transmission properties of a metafilm: with an application to a controllable surface composed of resonant particles, *IEEE Trans. Electromagn. Compat.* **47**, 853 (2005).
- [35] See Supplemental Material at <http://link.aps.org/supplemental/10.1103/PhysRevApplied.11.054012> for geometric parameters, equivalent electric admittance, and magnetic impedance of meta-atoms, the electric and magnetic responses of meta-atoms with varied spacer thicknesses, and the feature verifications of Airy beams based on HMS.
- [36] M. V. Berry and N. L. Balazs, Nonspreading wave packets, *Am. J. Phys.* **47**, 264 (1979).
- [37] G. A. Siviloglou, J. Broky, A. Dogariu, and D. N. Christodoulides, Observation of Accelerating Airy Beams, *Phys. Rev. Lett.* **99**, 213901 (2007).
- [38] G. A. Siviloglou and D. N. Christodoulides, Accelerating finite energy Airy beams, *Opt. Lett.* **32**, 979 (2007).
- [39] J. Baumgartl, M. Mazilu, and K. Dholakia, Optically mediated particle clearing using Airy wavepackets, *Nat. Photon.* **2**, 675 (2008).
- [40] P. Polynkin, M. Kolesik, J. V. Moloney, G. A. Siviloglou, and D. N. Christodoulides, Curved plasma channel generation using ultraintense Airy beams, *Science* **324**, 229 (2009).
- [41] D. Abdollahpour, S. Suntsov, D. G. Papazoglou, and S. Tzortzakis, Spatiotemporal Airy Light Bullets in the Linear and Nonlinear Regimes, *Phys. Rev. Lett.* **105**, 253901 (2010).
- [42] P. Panagiotopoulos, D. G. Papazoglou, A. Couairon, and S. Tzortzakis, Sharply autofocused ring-Airy beams transforming into non-linear intense light bullets, *Nat. Commun.* **4**, 2622 (2013).
- [43] M. A. Ordal, L. L. Long, R. J. Bell, S. E. Bell, R. R. Bell, R. W. Alexander, and C. A. Ward, Optical properties of the metals Al, Co, Cu, Au, Fe, Pb, Ni, Pd, Pt, Ag, Ti, and W in the infrared and far infrared, *Appl. Opt.* **22**, 1099 (1983).
- [44] E. Perret, N. Zerounian, S. David, and F. Aniel, Complex permittivity characterization of benzocyclobutene for terahertz applications, *Microelectron. Eng.* **85**, 2276 (2008).
- [45] Z. Han, S. Ohno, Y. Tokizane, K. Nawata, T. Notake, Y. Takida, and H. Minamide, Thin terahertz-wave phase shifter by flexible film metamaterial with high transmission, *Opt. Express* **25**, 31186 (2017).
- [46] S.-W. Qu, W.-W. Wu, B.-J. Chen, H. Yi, X. Bai, K. B. Ng, and C. H. Chan, Controlling dispersion characteristics of terahertz metasurface, *Sci. Rep.* **5**, 9367 (2015).
- [47] S. Qu, H. Yi, B. J. Chen, K. B. Ng, and C. H. Chan, Terahertz reflecting and transmitting metasurfaces, *Proc. IEEE* **105**, 1166 (2017).